

Article

Modeling Surface Roughness and Flow of Gases in Threaded Connections to Analyze Sealing Performance

Wenqi Zhu ¹ , Yu Liang ² and Lv Zhao ^{2,3,*}¹ Baoshan Iron & Steel Co., Ltd., Shanghai 201908, China² Department of Mechanics, School of Aerospace Engineering, Huazhong University of Science and Technology, Wuhan 430074, China³ Hubei Key Laboratory of Engineering Structure Analysis and Safety Assessment, 1037 Luoyu Road, Wuhan 430074, China

* Correspondence: lvzhao@hust.edu.cn

Abstract: Oil casings and premium threaded connections play vital roles in the oil and gas extraction industry. The present work establishes an integrated modeling framework for the sealability assessment of premium threaded connections which can be easily implemented and employed by engineers. The framework incorporates a part-scale finite element analysis of the make-up process, a micro-scale simulation of the contact behavior, and a mechanism-informed gap flow model. It is found that complete sealing can be achieved when the contact pressure exceeds 1540 MPa for Gaussian rough surfaces presenting a roughness of 1.6 μm . The seal surface fit is revealed to be critical for sealing performance, as it slightly changes the optimum make-up torque (up to 4%) but significantly changes contact pressure (up to 22%). At an optimum make-up torque, the connection with the loosest seal surface tolerance fit is prone to gas leakage when considering an inlet pressure of 110 MPa. The proposed modeling framework can be extended to other types of threaded connections with metal–metal contact sealing.

Keywords: threaded connection; finite element analysis; metallic seal; gap flow model; surface roughness



Citation: Zhu, W.; Liang, Y.; Zhao, L. Modeling Surface Roughness and Flow of Gases in Threaded Connections to Analyze Sealing Performance. *Processes* **2024**, *12*, 574. <https://doi.org/10.3390/pr12030574>

Academic Editor: Albert Ratner

Received: 1 February 2024

Revised: 27 February 2024

Accepted: 5 March 2024

Published: 14 March 2024



Copyright: © 2024 by the authors. Licensee MDPI, Basel, Switzerland. This article is an open access article distributed under the terms and conditions of the Creative Commons Attribution (CC BY) license (<https://creativecommons.org/licenses/by/4.0/>).

1. Introduction

Oil casings play an important role in the oil and gas extraction industry. Premium threaded connections are widely used to construct long casings for the purpose of reaching deep oil. The sealability performance of such connection components is ensured by the metal–metal contact of the sealing surface. Note that inadequate design (tolerance fit) and use (make-up) of casing connections may lead to leakages and considerable economic losses [1].

The make-up process of premium threaded connections is an important step prior to service. This step not only ensures the integrity of the oil casing, but also gives rise to high contact pressure, preventing leakage through the sealing surface. The completion of the make-up process is generally determined based on the make-up torque value, but the optimum make-up torque is hard to identify in practice. On the one hand, make-up torque is strongly influenced by the tolerance range and machining error and, on the other hand, it cannot be directly correlated to the sealability of the premium connection [1]. The experimental identification of optimum torque necessitates the in-time monitoring of contact pressure on the sealing surfaces. Although this can be achieved by advanced ultrasonic techniques [2], the plastic strain cannot be probed during the make-up process and it may reach an unacceptably high level if only contact stress is used as the indicator of optimum make-up torque [3].

Numerical modeling and simulations are powerful alternatives used to assess the make-up process of premium threaded connections. With 2D finite element analysis, the make-up of premium connections was widely simulated by imposing a certain amount

of interference [4–6]. However, such treatment cannot reflect the real make-up process of the premium connection. Recently, 3D finite element simulations have become more and more widely used in assessing the performance of oil casing connections. A large number of works have been devoted to studying the evolution of contact stress during make-up and thermo-mechanical loading [7–11]. Nevertheless, except for our previous effort [3], there are no other works addressing the identification of optimum make-up torque. Moreover, most previous studies used coarse elements without evaluating mesh convergence. Note that a sufficiently fine mesh is required to accurately probe contact pressure on sealing surfaces.

Although contact pressure is the key factor determining the sealability of a premium connection, how to quantitatively assess sealing performance remains an important issue. There exist two widely used approaches; one is a phenomenological law and the other is a mechanism-based model. Based on the results of gas-tight tests, Murtagian et al. [12] and Xie et al. [13] proposed sealing indices involving the integration of contact pressure along the sealing path. Correspondingly, sealing criteria incorporating pressure influence, seal ring diameter, leakage rate threshold, and fitting parameters were defined. This phenomenological law exhibits a simple form and ease of application but omits the underlying physics of leakage. Moreover, the influence of surface roughness on sealability cannot be considered. Note that the plastic deformation of rough surfaces and surface morphology significantly affect the fluid leakage of metallic seals, as demonstrated by Fischer et al. [14] and Ernens et al. [15], respectively.

Indeed, roughness may lead to the formation of leakage channels between the seal surfaces, and then fluid will flow through the channels due to the pressure difference between the two ends [15]. In this sense, two aspects need to be solved to build a mechanism-based sealing criterion. The first is contact analysis between rough seal surfaces. The generation of surface roughness can be achieved through statistical models [16,17], fractal models [18,19], and deterministic models [20,21]. The contact of rough surfaces can be solved by either theoretical calculation [16,20] or numerical simulation [22]. The combination of a deterministic model and numerical simulation can be regarded as a more flexible and easy-to-implement tool with which to approach real contact behavior between rough seal surfaces. The vital role of contact analysis lies in rendering an accurate leakage channel [22,23] for the following investigation of fluid flow, i.e., the second aspect for building a mechanism-based sealing criterion. The fluid leakage rate can be estimated by the average flow model [24] and percolation theory [25]. The average flow model first considers fluid flow between plates, and then the influence of surface roughness is introduced via a flow factor (<1). It can be easily implemented and used in the assessment of sealability. Percolation theory relies on first treating the rough surfaces in contact as a porous medium and identifying leakage channels, and then calculating the rate of fluid flow through the channels. This theory captures the physics of fluid flow behavior, but its applicability to addressing engineering issues needs further approval.

The present work aims to build an integrated modeling framework for the sealability assessment of premium threaded connections that can be easily implemented and used by engineers. This framework incorporates 3D finite element analysis of the make-up process, based upon which the optimum make-up torque is determined, and a gap flow model which is capable of assessing the fluid leakage rate in the case of complex contact pressure distribution. The framework is successfully applied to evaluate the sealability of premium connections with different tolerance fits.

2. Modelling and Simulation

2.1. Finite Element Simulation of Connection Make-Up

The premium threaded connection model was built with Ansys APDL, which allows for parametrically generating the geometries with different tolerances (see Figure 1a). Note that the detailed dimensions of the model cannot be provided due to the confidentiality issue. Then, the model was discretized with approximately two million hexahedron

elements. The meshed geometry is shown in Figure 1b. The threads present a characteristic element size of 200 μm and the sealing components (seal surface and torque shoulder) present a characteristic element size of 100 μm . This mesh size has been selected based on the balance between the accuracy and computational cost, as shown in our related work [3]. The material used for the threaded connection is P110 steel. Uniaxial tensile tests were performed at room temperature (25 °C) to obtain the mechanical properties of the material. The Young's modulus (210 GPa) and yield strength (873 MPa) were extracted directly from the experimental results, and the hardening stage was fitted with an exponential law ($\sigma = 1350e^{0.07}$).

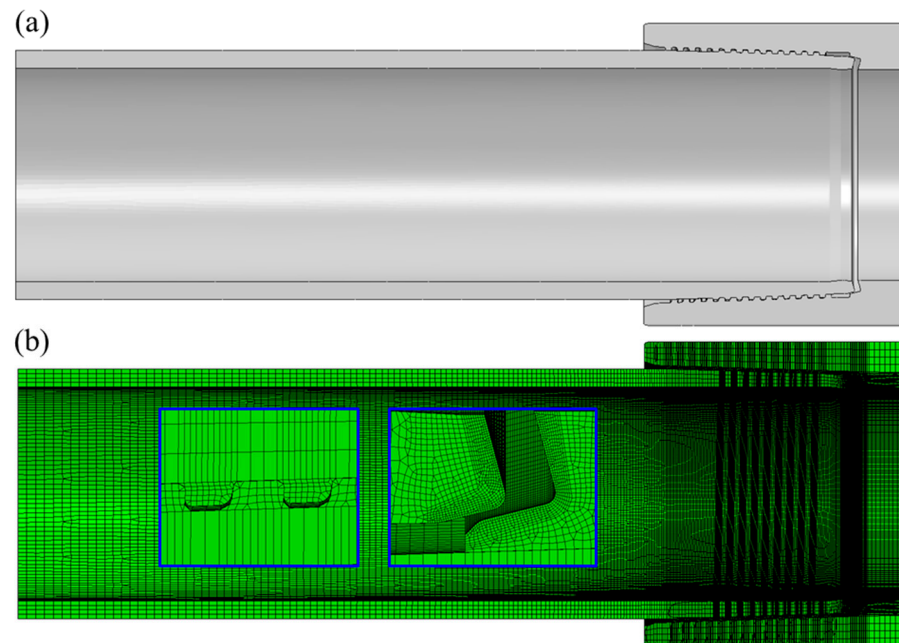


Figure 1. Geometric model (a) and mesh (b) of the premium threaded connection for finite element simulations. The inserts in (b) show the element refinement for the threads and the sealing components.

The simulations of the make-up process of the premium connection were carried out with Abaqus standard (V6.12), where the finite slide scheme and a friction coefficient of 0.05 were adopted in the contact algorithm. It should be noted that Abaqus explicit could also be used to conduct the simulation of the make-up process, but the computation time was extremely long based on our preliminary trial, due to the fact that the fine elements prescribe a super small time increment to maintain the stability.

Two reference points were generated and assigned to the pin and the box, respectively, on which the boundary conditions were applied. All the degrees of freedom for the reference point of the box were blocked, and an angular velocity of 4 rad/s was applied to the reference point of the pin to enable the make-up. The geometrical non-linearity was taken into account in the simulations, considering the possible generation of large plastic strain.

In order to probe the influence of tolerance fit on the performance of the premium connection, four simulation cases were considered; one with nominal dimensions, one with the loosest thread fit, one with the loosest seal surface fit, and one with the tightest seal surface fit. The optimum make-up torque, the stress and strain states upon make-up completion, and the sealing performance will be compared based on the simulation results.

2.2. Framework of Leakage Rate Assessment

The leakage rate was assessed with a framework incorporating macroscopic and mesoscopic finite element analyses, computational fluid dynamics (CFD) simulations, and

an analytical gap flow model. The whole framework is shown in Figure 2. First, a finite element simulation of the make-up of the premium connection was performed (Section 2.1), based upon which the optimum make-up state (make-up torque) was identified. Subsequently, the contact pressures on the sealing surface were extracted, which served as the key input parameters for the sealing performance assessment. Afterwards, a mesoscopic contact model was built to assess the gap between rough surfaces and its evolution with the applied contact pressure. The gap distribution was then imported into a CFD model to calculate the flow factor, i.e., a flow rate reduction coefficient induced by the surface roughness. Finally, an average gap flow model was established and numerically implemented, allowing for the evaluation of the sealability of the premium connection.

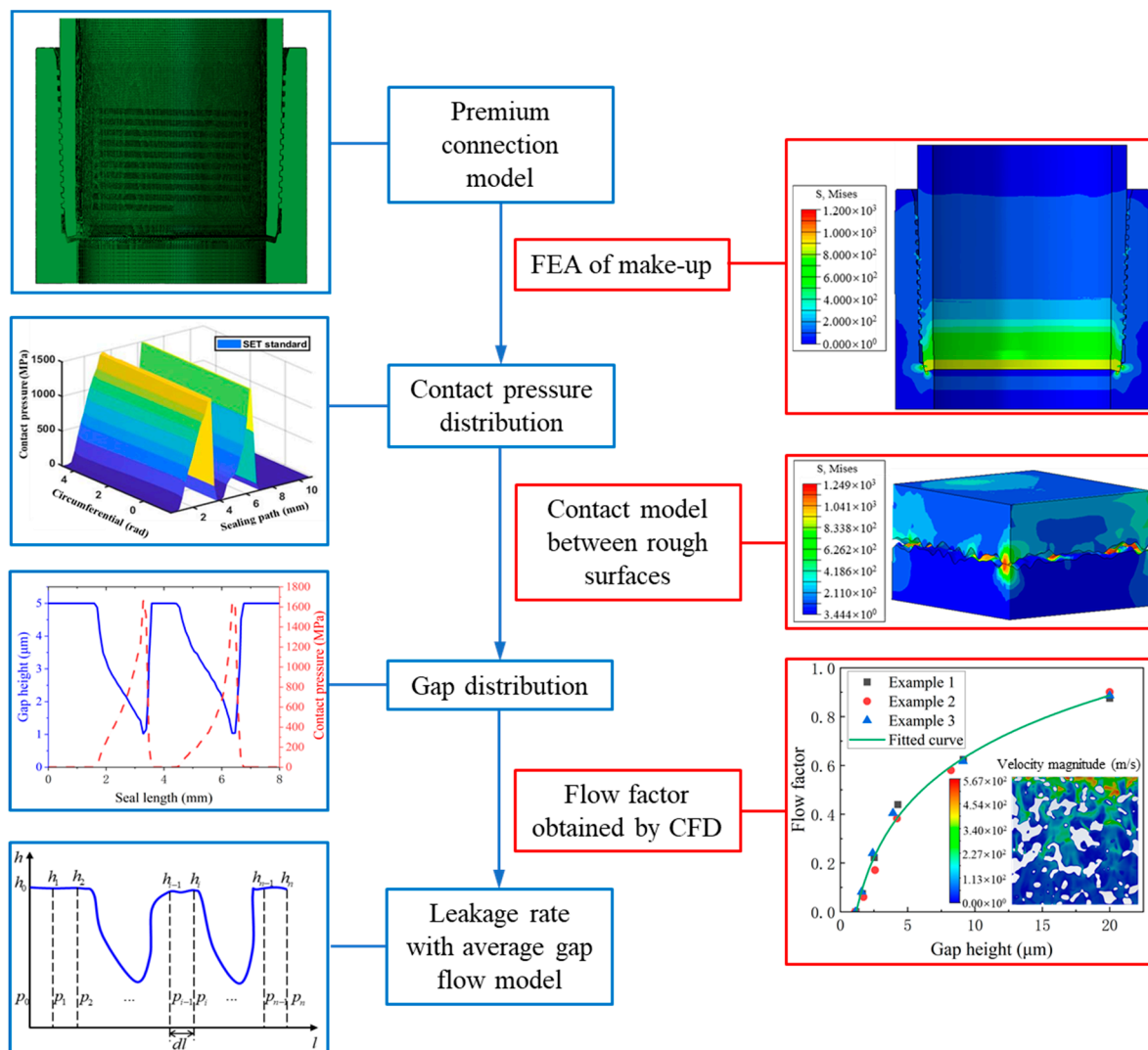


Figure 2. Flow chart of the framework for leakage rate assessment.

The aforementioned framework exhibits several advantages. First, it allows for the assessment of the optimum make-up state and hence the sealing ability for different tolerance fits. Second, the framework considers the physical aspect of the leakage through the gap flow model, in contrast to other works that assess the sealability with only the contact pressure. Third, the influence of the surface roughness is considered in the leakage flow calculation, so that the machining quality of the premium connection can be assessed. The details of the mesoscopic contact model, the CFD simulations, and the average gap flow model will be presented in Section 3.2.

3. Results and Discussion

3.1. Identification of Optimum Make-Up State

The contact pressure is a key indicator of the sealing performance of the premium connection, and it will be used as the input parameter for the assessment of leakage rate. Moreover, the contact pressure and its evolution are important elements for identifying the optimum make-up torque. Figure 3 shows a typical contact pressure distribution on the sealing surface (composed of the seal surface and the torque shoulder) obtained from the simulation of the make-up process. Two contact pressure peaks can be observed along the sealing path, one on the torque shoulder segment and the other on the seal surface segment (Figure 3b). Moreover, the contact pressure appears to be nearly constant along the circumferential path, although the helical characteristic of the threads is considered in the model. In this sense, it will be sufficient to probe the contact pressure distribution along the sealing path (Figure 3c).

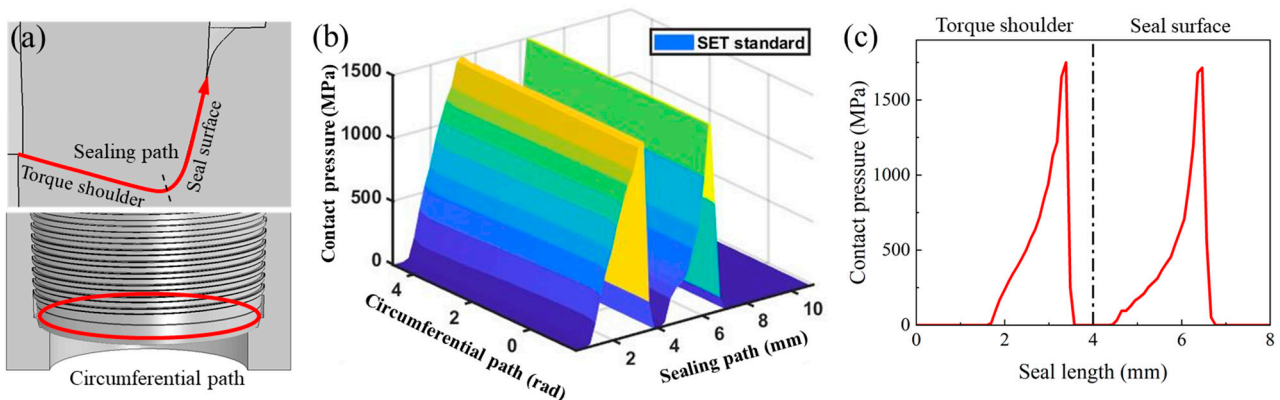


Figure 3. Definition of sealing path and circumferential path (a), typical contact pressure distribution on the sealing surface (b), typical contact pressure distribution along the sealing path (c).

For the make-up process of the premium connection, it is important to determine the optimum make-up torque. Figure 4a shows the theoretical shape of the make-up torque [26], involving three distinct stages of the torque evolution. The first stage starts with the thread interference, giving rise to a linear increase of the torque from zero (stage AB); the second stage begins with the seal surface interference leading to a slightly faster linear increase of the torque (stage BC); the third stage is characterized by a much higher slope of the torque increase due to the shoulder interference (stage CD). In general, an optimum torque value occurs within the third stage. Figure 4b presents the make-up torque curves for the four tolerance fits obtained from the finite element simulations. It can be seen that the numerically resolved torque curves are in good agreement with the theoretical analysis. Therefore, the torque partition between the threads (T_{th}), the seal surface (T_{se}), and the shoulder (T_{sh}) can be determined using the approach shown in Figure 4a. When comparing the torque curves obtained from the different simulation cases, it is found that the thread tolerance fit significantly affects the stage AB, whereas the seal surface tolerance fit has only a very slight influence on the stage BC.

To determine the optimum make-up torque, the balance between the contact pressure and the plastic deformation of the connection should be considered. Figure 5 shows the evolutions of the maximum contact pressure and the maximum plastic strain as a function of the make-up torque for the four considered tolerance fits. For all cases, the peak contact pressure first quickly rises and then tends to flatten or even drop, whereas the peak plastic strain (especially for the shoulder) exponentially increases with the increase of the make-up torque. Considering the compromise of a sufficiently high contact pressure and a low plastic strain ($\approx 1\%$) of the sealing parts, the optimum make-up torques are determined to be 3131 N·m (Figure 5a), 2398 N·m (Figure 5b), 3003 N·m (Figure 5c), and 3255 N·m (Figure 5d) for the four tolerance fits, respectively. The peak contact pressure corresponding

to the optimum make-up torque is higher than 1500 MPa and is close to the largest value for the cases of the nominal dimensions, the loosest thread fit, and the tightest seal surface fit, whereas it presents a much lower value for the loosest seal surface fit, especially for the seal surface segment. To further increase the contact pressure for this case, the make-up torque needs to be elevated, but this will in turn trigger a significant increase of the plastic strain of the shoulder.

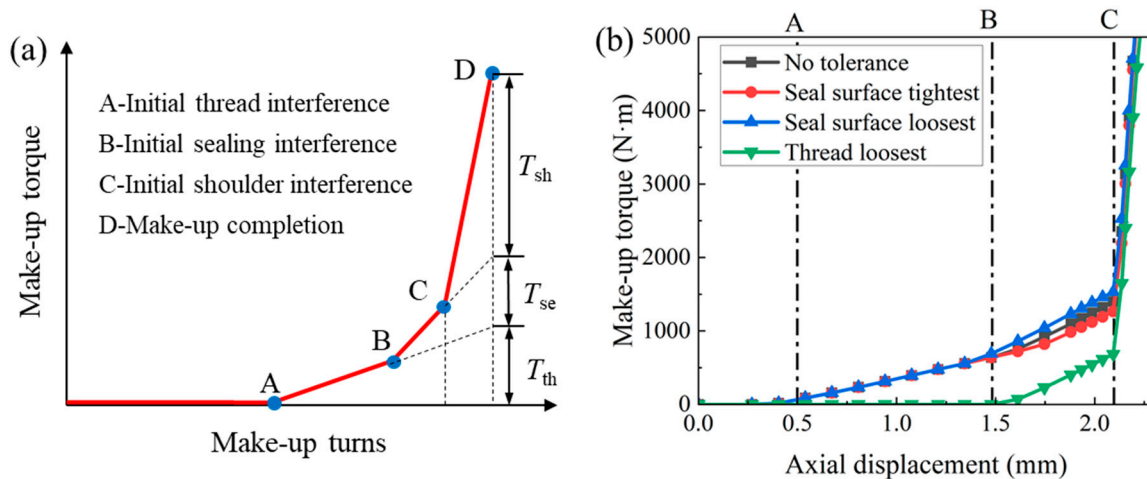


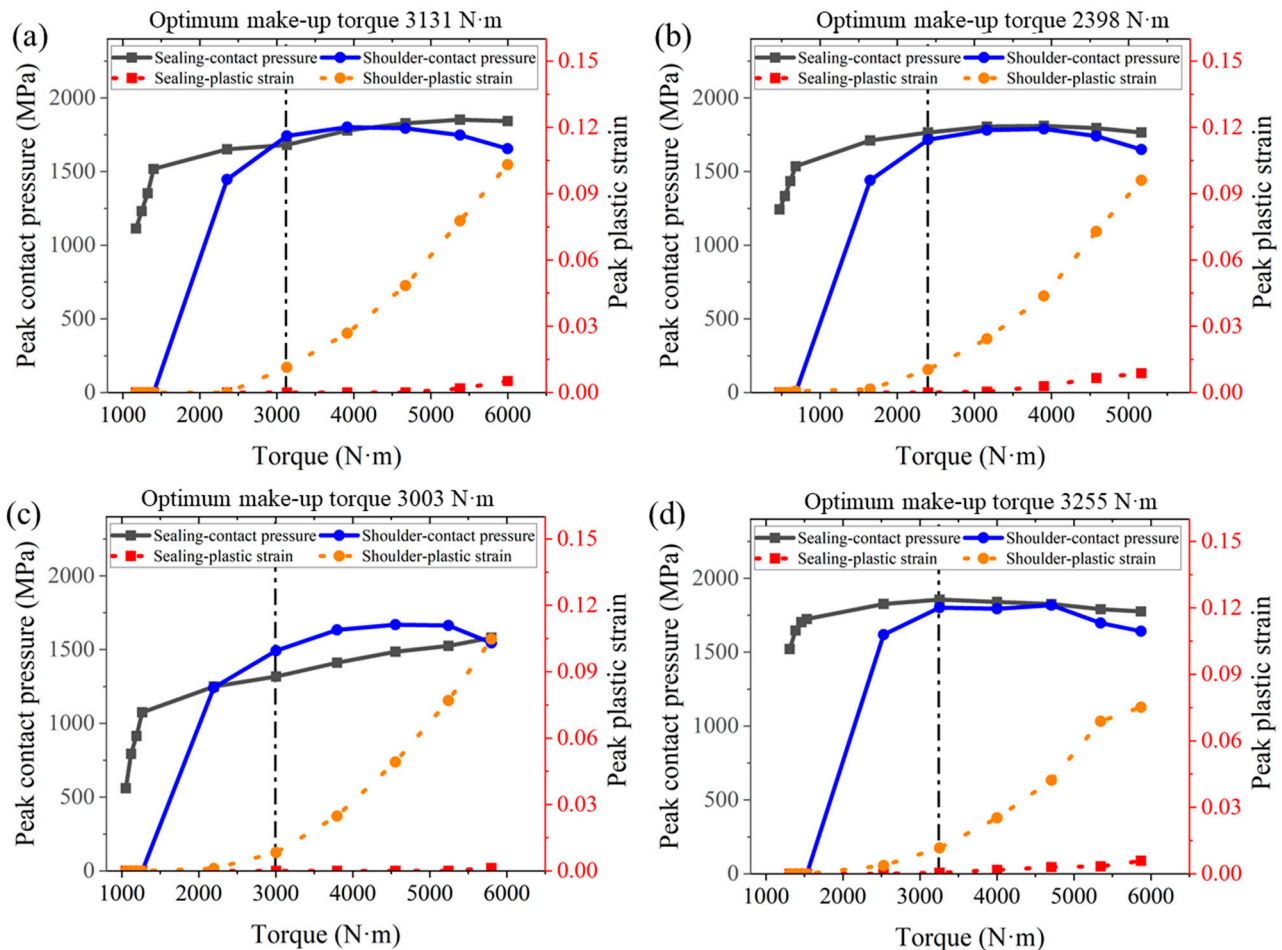
Figure 4. Theoretical shape of the make-up torque (a), make-up torque curves for different tolerance fits obtained with the finite element simulations (b).

From Figure 5, it can be seen that the tolerance fit of the threads significantly affects the optimum torque, whereas the tolerance fit of the seal surface has only a slight influence. To disclose the reason behind this, the torque partition upon the make-up completion (i.e., at the optimum make-up torque) for the four tolerance fits is analyzed and presented in Table 1. It is found that the shoulder torque is almost the same for all cases. This is due to the fact that the optimum make-up torque has been selected with the same shoulder plastic strain. For the case of the nominal dimensions, the shoulder torque occupies 53% of the total torque, the thread torque 33%, and the seal surface torque only 15%. For the loosest thread fit, the thread torque decreases by 72% compared to the case of the nominal dimensions, therefore leading to a marked reduction of the total torque (by 23%). For the loosest and the tightest seal surface fits, the seal surface torque changes by -27% and $+27\%$, respectively. However, this variation does not significantly affect the total torque (by -4% and $+4\%$) as the contribution of the seal surface torque is relatively low.

The contours of the von Mises stress and the equivalent plastic strain at the optimum make-up torque are shown in Figure 6. The legends are unified for the four cases to enable a direct comparison. It is observed that the stress and strain fields of the sealing components (i.e., the seal surface and the torque shoulder) are quite similar between the cases of the nominal dimensions and the loosest thread fit (Figure 6a,b). This can be explained by the close seal surface torque and the shoulder torque between the two conditions (Table 1). Regarding the two seal surface tolerance fits, the loosest interference mitigates the stress and strain levels of the sealing components while the tightest interference enhances them (Figure 6c,d). These are also in line with the changes in the maximum contact pressure with respect to the case of the nominal dimensions, as can be seen in Figure 5c,d.

Table 1. Make-up torque partition for the four different tolerance fits.

Cases	No Tolerance	Loosest Thread Fit	Loosest Seal Surface Fit	Tightest Seal Surface Fit
T_{th} (N·m)	1021	286	1021	1021
T_{se} (N·m)	460	460	333	585
T_{sh} (N·m)	1650	1652	1649	1649
T_{tot} (N·m)	3131	2398	3003	3255

**Figure 5.** Determination of the optimum make-up torque for the cases of the nominal dimensions (a), the loosest thread fit (b), the loosest seal surface fit (c), and the tightest seal surface fit (d), based on the balance between maximum contact pressure and plastic deformation.

In summary, this section investigates the make-up process of the premium threaded connection involving different tolerance fits. The optimum make-up torque has been identified for each case under the balance between the contact pressure and the plastic strain. The thread tolerance fit is found to significantly affect the torque curve but exhibits little influence on the contact pressure or the stress and strain fields of the sealing components. In contrast, the seal surface tolerance fit is revealed to slightly change the torque curve but strongly influence the contact pressure and the stress and strain fields of the sealing components. The simulation results at the optimum make-up torque will be used as the inputs for the assessment of the leakage rate in Section 3.3.

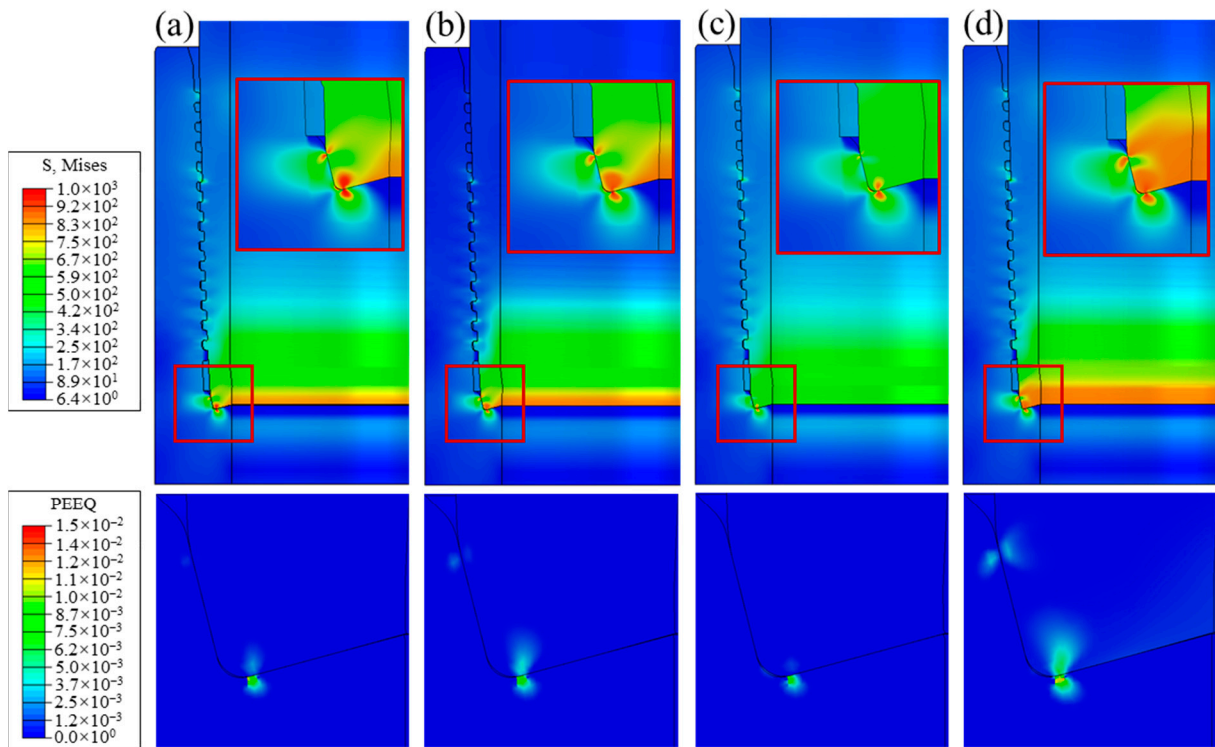


Figure 6. Contours of the von Mises stress and plastic deformation at the optimum make-up torque for the cases of the nominal dimensions (a), the loosest thread fit (b), the loosest seal surface fit (c), and the tightest seal surface fit (d). The unit for the stress is MPa.

3.2. Leakage Rate Calculation Model

To improve the prediction accuracy of sealability, the physics of the leakage should be included when establishing a predictive model. The present work considers the fluid flow between rough surfaces in the assessment of leakage of the premium threaded connection, given that the surface of the sealing parts exhibits a certain roughness. The height coordinate of the rough surface is assumed to follow the Gaussian distribution:

$$p(z) = \frac{1}{\sqrt{2\pi}} e^{-\frac{z^2}{2}}. \quad (1)$$

The x , y , and z represent the two in-plane and the one out-of-plane directions of the contact surface, as can be seen in Figure 7. The following self-correlation function was used to establish the correlation between two points on the rough surface:

$$p(d) = R_q^2 e^{-\left(\frac{d}{L_c}\right)^2}, \quad (2)$$

where d represents the distance between the two points, L_c the self-correlation length, and R_q the root-mean-square (RMS) roughness of the surface. Combining the above two equations, the rough surface can be expressed with the amplitude square matrix:

$$z(x, y) = \sum_{i=-M}^M \sum_{j=-N}^N w(i, j) g(x + i, y + j) \quad (3)$$

$$w(i, j) = \frac{2R_q}{L_c \sqrt{\pi}} e^{-\frac{2(i^2 + j^2)}{L_c^2}}, \quad (4)$$

where M and N are the numbers of points along the x and y axes, and $g(x + i, y + j)$ is a Gaussian random matrix with an average of 0 and a variance of 1.

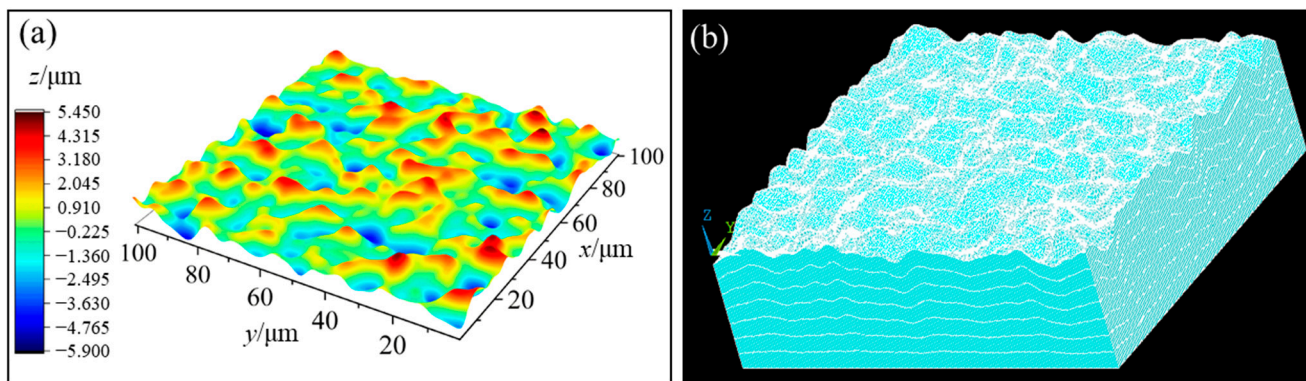


Figure 7. Generation of rough surfaces for the mesoscale contact simulations. Three-dimensional (3D) rough surface generated by the self-correlation function (a), the finite element mesh of the solid model incorporating the rough surface (b).

According to the measurements of the real premium connections, the roughness of the sealing surface is $1.6 \mu\text{m}$. Taking the self-correlation length of $4 \mu\text{m}$, a rough surface of $100 \times 100 \mu\text{m}$ was generated, as shown in Figure 7a. Note that the size of $100 \mu\text{m}$ was used to be consistent with the element size of the sealing surface used for the simulation of the make-up process. To further perform contact analysis between rough surfaces, a finite element model incorporating the rough surface was created, as presented in Figure 7b. The thickness of the model is $30 \mu\text{m}$, the element size on the xy plane is about $0.4 \mu\text{m}$, and the total element number is 420,000.

Two models were generated following the aforementioned steps to simulate the contact between two rough surfaces. The simulation was performed in Abaqus standard. The material properties are the same as those used for the part-scale simulations (see Section 2.1). The lower block was fixed and the upper block moved vertically downwards. As the generation of the roughness involves a randomness, three sets of models were created and simulated to verify the validity of the rough surface construction. The simulation results are shown in Figure 8. It can be seen that the nominal contact pressure first slowly increases with the move-down displacement of the upper block due to a small contact area. When the contact area enlarges, the nominal contact pressure also rapidly rises. During the contact of the rough surfaces, the local contact stress is high and a large plastic strain is created. Meanwhile, as long as there exist contact-free sunken areas, gaps between the rough surfaces are retained. If these gaps are interconnected, leakage channels will be formed. It is noteworthy that very high nominal contact pressure levels are obtained (see Figure 8b). On the one hand, the material mainly deforms in a compressive manner in the contact model and therefore can bear a large stress before failure. On the other hand, no failure criterion is incorporated in the model. Nevertheless, the high contact pressure level is only used for fitting the gap height–contact pressure relationship (Figure 8c).

In order to calculate the leakage rate, the average gap height between the rough surfaces under any given nominal contact pressure needs to be resolved. To this end, the z coordinates of all surface points are extracted and the average value is calculated, defining the z coordinate of the reference plane of the rough surface. The average gap height is therefore obtained as the difference between the z coordinates of the upper and lower reference planes. This calculation procedure is applied for each nominal contact pressure, and the gap height evolution with the contact pressure is therefore established (see Figure 8c).

The interconnected gap between the rough surfaces provides the flow path for the fluid. The leakage channels can be constructed with the contact simulation results, specifically the coordinates of the rough surfaces during the contact process. Figure 9 shows the potential leakage channels between the two rough surfaces under different nominal contact pressures. It can be seen that the blocked area (in black) enlarges with increasing nominal contact pressure. Based on the results obtained from three independent contact simulations, it is

found that no interconnected gap between the rough surfaces exists when the nominal contact pressure exceeds 1540 MPa. The latter can therefore be regarded as the threshold value of complete sealing.

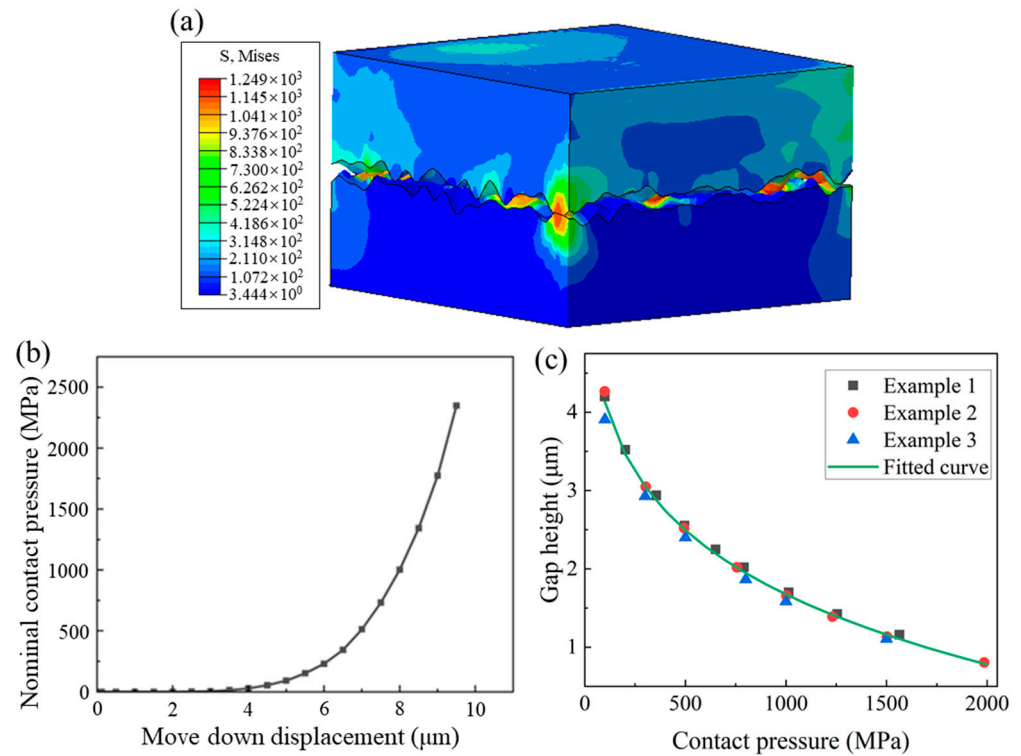


Figure 8. Contour of the von Mises stress during the contact between the rough surfaces (a), nominal contact pressure vs. move-down displacement (b), evolution of the gap height between the rough surfaces with the increase of the contact pressure (c). The unit for the stress is MPa.

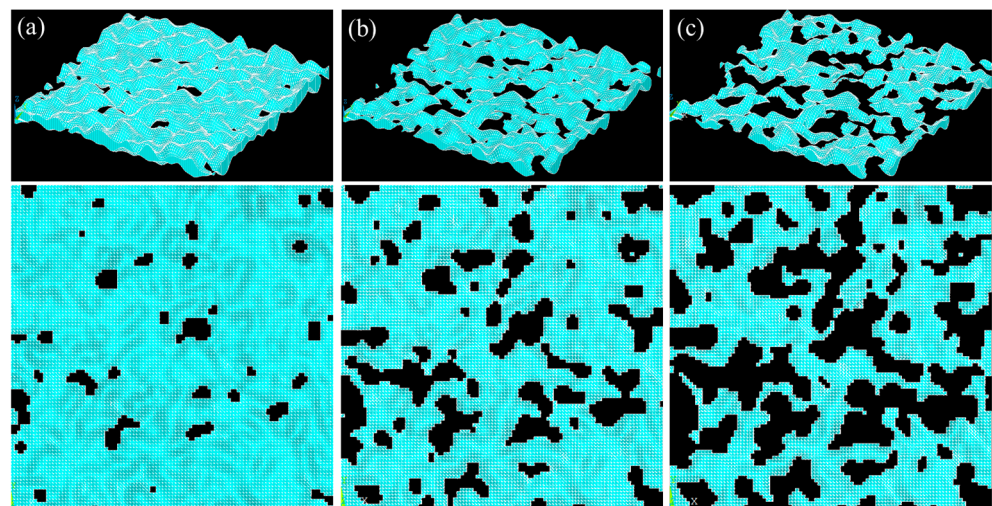


Figure 9. Blocked leakage channel (black area) at the contact pressure of 99 MPa (a), 494 MPa (b), and 1002 MPa (c).

It has been proposed in previous literature that the flow rates between two rough surfaces (presenting a gap of h between the reference planes) and between two smooth plates (with a gap of h) can be related with:

$$Q_s = \varphi Q_p \quad (5)$$

$$\varphi = f(R_q, h), \quad (6)$$

where φ is the flow factor, representing the reduction effect of the surface roughness on the flow rate. This factor is dependent on the roughness R_q and the gap h . The flow factor will be adopted in the present work.

For the case of fluid flow between smooth plates, the steady flow rate of incompressible fluid under a certain pressure difference reads:

$$Q = \frac{bh^3}{12\mu l} \Delta p, \quad (7)$$

where b is the width of the plate, l the length, μ the viscosity of the fluid, and Δp the difference between the inlet and outlet pressures. Considering the fact that the pressure inside the oil casing can reach over 100 MPa, the pressure will drop by nearly 1000 times when the fluid leaks to the ambient. Therefore, the change of the fluid density with the pressure cannot be ignored. In the present work, the ideal gas state equation was employed to establish the relation between the density and the pressure of the fluid as follows:

$$\begin{cases} pv = nRT \\ \rho = \frac{m}{v} \end{cases} \Rightarrow \rho = \frac{m}{nRT} p, \quad (8)$$

where v is the gas volume, R the gas constant, T the temperature, ρ the gas density, m the gas mass, and n the quantity of gas. Combining Equations (7) and (8), the mass flow of the gas between smooth plates is expressed as:

$$\dot{m} = Qp = \frac{bh^3}{12\mu l} \frac{m}{nRT} \bar{p} \Delta p. \quad (9)$$

When the flow factor is considered, the mass flow of the gas between rough surfaces can be written as:

$$\dot{m} = \varphi(h) \frac{bh^3}{12\mu l} \frac{m}{nRT} \bar{p} \Delta p. \quad (10)$$

The determination of the flow factor $\varphi(h)$ is carried out as follows. Under a given gap height, the flow rate between smooth plates is calculated with Equation (7), and the flow rate between rough surfaces is obtained with CFD simulation (Ansys Fluent). The leakage channels obtained by the contact simulation between rough surfaces (Figure 9) were imported to the Fluent software (2023R1). The settings of the analytical model and the simulation are the same: the size of the flow area is $100 \times 100 \mu\text{m}$, the pressure difference is 5000 Pa, and the fluid is air with viscosity of $1.79 \times 10^{-5} \text{ kg}/(\text{m}\cdot\text{s})$. The mass flow for the inlet and outlet in the direction perpendicular to the leakage path was zero. The fluid velocity field obtained with Fluent is shown in Figure 10a. It can be seen that the flow behavior between rough surfaces is quite complex. Based on the flow rates obtained by the two methods, the flow factor as a function of the gap height is obtained (see Figure 10b) and fitted with:

$$\varphi(h) = 6.967h^{0.04218} - 7.019. \quad (11)$$

It can be seen in Figure 10b that the flow factor nonlinearly evolves and tends to saturate to 1, i.e., the theoretical upper limit of the flow factor. Indeed, when the gap height is sufficiently large, the influence of the surface roughness on the flow behavior will gradually vanish and the CFD results will collapse to the gap flow model involving smooth plates. The nonlinear evolution could be explained by the fact that the contact behavior between the two rough surfaces significantly affects the flow channel (see Figure 9) when the gap height is small ($<5 \mu\text{m}$).

In a nutshell, a leakage rate calculation model is established combining contact simulations between rough surfaces, an analytical fluid flow model involving smooth plates, the ideal gas state equation, and CFD simulations. This model needs to be properly imple-

mented to consider complex contact pressure distribution along the sealing path, as will be addressed in the following section.

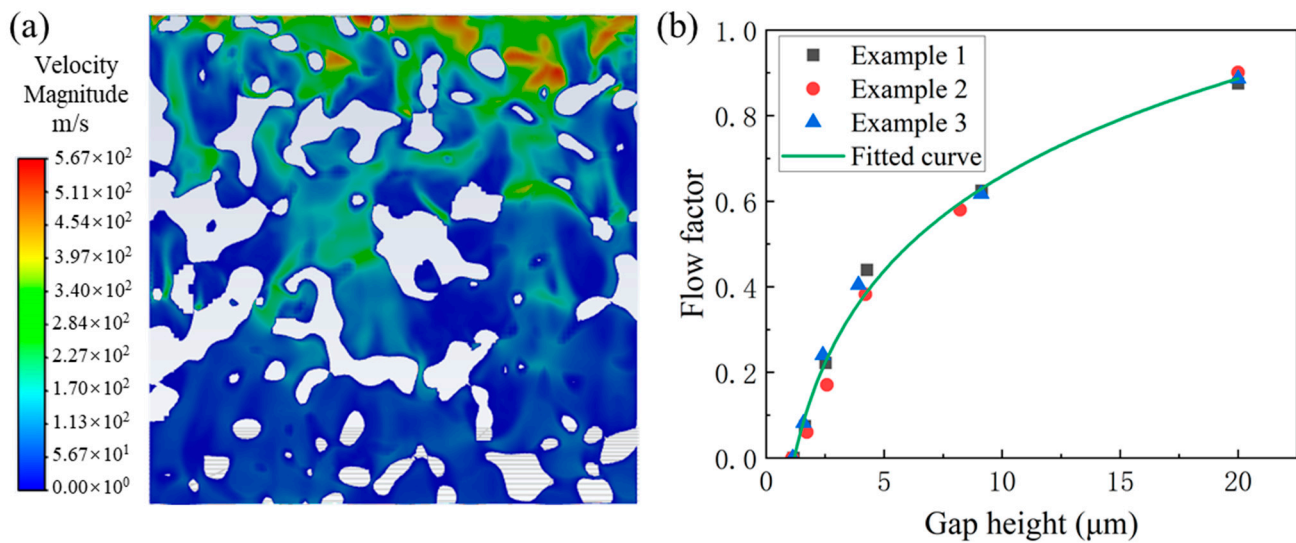


Figure 10. Determination of the flow factor. Representative CFD simulation result showing the fluid velocity contour between rough surfaces (a), evolution of the flow factor as a function of the gap height (b).

3.3. Sealing Performance of Premium Connection

It has been shown in Section 3.1 that the contact pressure significantly varies along the sealing path (see Figure 3c). This will, in turn, lead to steep variations of the gap height, in particular a very narrow orifice at the location of the maximum contact pressure, as shown in Figure 11a. In previous works, researchers have attempted to use the averaged contact pressure along the sealing path (i.e., averaged gap height) to calculate the leakage rate with Equation (10). However, this method may lead to important errors, as will be shown later in this section. To accurately compute the flow rate between gaps with a varying height, the leakage path is discretized by n segments, and each segment has a length of dl (see Figure 11b). Analogous to a differential issue, the height variation in each segment can be ignored when dl is sufficiently small, so all the segments can be regarded as plates, as shown in Figure 11c.

Therefore, the mass flow rate for each segment can be calculated by:

$$\dot{m} = \varphi(h_i) \frac{bh_i^3}{12\mu l} \frac{m}{nRT} \frac{p_{i-1} + p_i}{2} (p_{i-1} - p_i). \quad (12)$$

Considering the mass flow conservation through each segment, n equations can be established for the n segments, where the pressures at the $n - 1$ sections (p_1, p_2, \dots, p_{n-1}) and the mass flow rate \dot{m} in the whole leakage path are unknown. Using the Newton iterative algorithm, the n equations can be solved. It is noteworthy that the evolution of the viscosity with the pressure is neglected in the model, as the variation is generally not significant. On the other hand, such simplification leads to conservative predictions as the viscosity is larger at higher pressures, and the present work adopts the gas viscosity at the ambient pressure.

To validate the discretized realization of the leakage flow model and prove its superior accuracy compared to the averaged gap model, three cases are considered, one with a constant gap height and two with cosine gap height variations, the averaged gap heights all being 2 μm. The settings are as follows: the leakage channel length is 4 mm, the pressure difference is 0.1 MPa, and the fluid is air. The comparison between the predictive models and the CFD simulations is given in Table 2. When the flow domain is planar, the results of

the three approaches are nearly the same. However, when the gap height is variable, the averaged gap flow model leads to results that deviate from the discretized flow model and the CFD simulation, which give very close results. In addition, the deviation is augmented with the increase of the variation amplitude of the gap height.

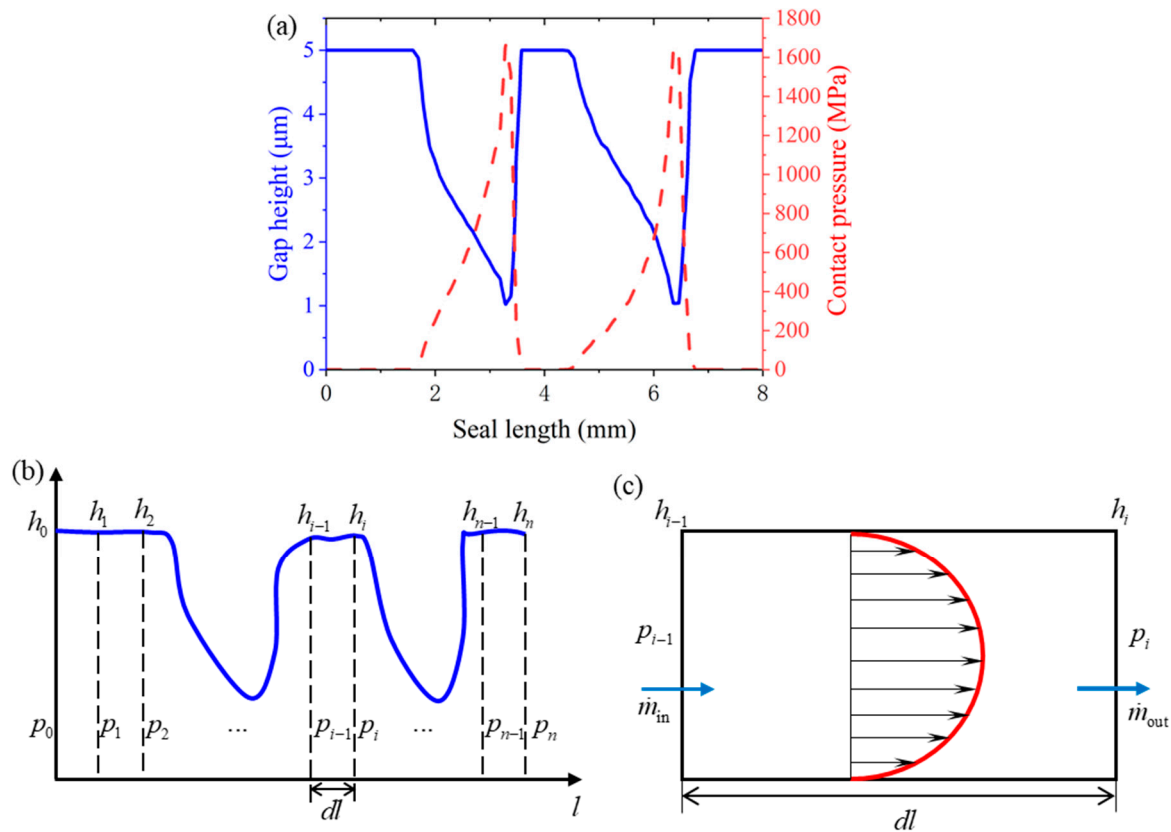


Figure 11. Variations of the gap height and the contact pressure along the leakage path (a), discretization of the leakage path for the calculation of fluid leakage rate (b) with the gap flow model applied to the infinitesimal leakage path (c).

Table 2. Comparison of mass flow rate between different calculation approaches.

Gap Height (μm)	Averaged Gap (Equation (10)) (kg·s ⁻¹)	Discretization (Equation (12)) (kg·s ⁻¹)	Fluent (kg·s ⁻¹)
2	1.6328×10^{-6}	1.6328×10^{-6}	1.6453×10^{-6}
$2 + \frac{1}{2} \cos(2\pi \frac{x}{l})$	1.6328×10^{-6}	1.3474×10^{-6}	1.3507×10^{-6}
$2 + \frac{3}{2} \cos(2\pi \frac{x}{l})$	1.6328×10^{-6}	1.6134×10^{-7}	1.6310×10^{-7}

With the discretized gap flow model, the sealing performances of the four tolerance fits are assessed by importing the corresponding contact pressure distributions upon the make-up completion. The inlet pressure is set to 110 MPa and the outlet pressure to 0.1 Mpa, and the fluid is air with a viscosity of 1.79×10^{-5} kg/(m·s). The calculation results are shown in Table 3. Except for the loosest seal surface fit, the leakage is strictly suppressed for the other three conditions. This is due to the fact that the maximum contact pressures of these three tolerance fits are higher than the threshold value of complete sealing (1540 MPa). From Figure 5c, it can be seen that one should compromise on the plastic strain to increase the contact pressure (i.e., enhance the sealing performance) for the loosest seal surface fit.

Table 3. Gas leakage rates for different tolerance fits.

Cases	No Tolerance	Loosest Thread	Loosest Seal Surface	Tightest Seal Surface
Leakage rate ($\text{m}^3 \cdot \text{s}^{-1}$)	0	0	9.0702×10^{-3}	0

In summary, the proposed gap flow model can be used to investigate the leakage rate of the premium threaded connection. It is found that the connection with insufficient seal surface interference is prone to gas leakage when the internal pressure is high.

The proposed integrated modeling framework represents an advancement for evaluating the sealability of the premium connections. It can be extended to other types of threaded connections with metal–metal contact sealing. The flow factor needs to be recalculated to consider other flow forms involving different contact surface morphologies. Nevertheless, one should be aware of the assumptions and simplifications in the establishment of the gap flow model. Future works are needed to improve the model’s applicability in real engineering practices.

- Although the fluid compressibility is considered in the flow rate, the evolutions of the fluid density, the pressure, and the temperature with the Mach number are omitted. Note that, in the case of a high pressure drop of gas, the flow velocity may reach or exceed the speed of sound. Moreover, gases with high temperatures and high pressures cannot be addressed with the current gap flow model due to the use of the ideal gas state equation.
- Molecular effects could become dominant for the gas flow between rough surfaces with few microns; the flow factor obtained with the CFD simulations may need to be rectified.
- The contact model between rough surfaces only takes into account micro-scale surface morphology; to further improve the accuracy of the model, the submicron surface structure needs to be considered.
- The sealing surface of the connection is mainly finished with lathe machining, so the surface morphology may deviate from the Gaussian distribution. The experimentally measured surface morphology data can be incorporated in the contact analysis between rough surfaces.

4. Conclusions

The present work has proposed an integrated modeling framework for assessing the sealing performance of the premium threaded connection with different tolerance fits. First, finite element simulations of the make-up process have been performed and the corresponding optimum make-up torques have been identified. Then, a gap flow model has been established. Finally, the model has been employed to assess the leakage rate for the considered tolerance fits. The main conclusions are as follows:

1. The seal surface tolerance fit changes the optimum make-up torque very slightly (up to 4%) but significantly changes the contact pressure (up to 22%) of the sealing components. The maximum contact pressures are 1681 MPa (no tolerance), 1317 Mpa (loosest seal surface), and 1855 MPa (tightest seal surface).
2. A leakage rate calculation model is established, and it is found that a complete sealing could be achieved when the contact pressure exceeds 1540 MPa for Gaussian rough surfaces presenting a roughness of 1.6 μm .
3. At the optimum make-up torque, the connection with the loosest seal surface tolerance fit is prone to gas leakage (i.e., leakage rate of $9.0702 \times 10^{-3} \text{ m}^3 \cdot \text{s}^{-1}$) when considering an inlet pressure of 110 MPa. To enhance the sealing performance for such a case, the plastic strain level should be compromised at the cost of the reusability of the premium connection.

Author Contributions: Conceptualization, L.Z.; Methodology, W.Z. and Y.L.; Formal analysis, W.Z. and Y.L.; Investigation, W.Z. and Y.L.; Writing—original draft, W.Z. and Y.L.; Writing—review & editing, L.Z.; Funding acquisition, L.Z. All authors have read and agreed to the published version of the manuscript.

Funding: This research was funded by the Fundamental Research Funds for the Central Universities (grant number 2021XXJS116).

Data Availability Statement: The data that support the findings of this study are available from the corresponding author upon reasonable request.

Conflicts of Interest: Author Wenqi Zhu was employed by the company Baoshan Iron & Steel Co., Ltd. The remaining authors declare that the research was conducted in the absence of any commercial or financial relationships that could be construed as a potential conflict of interest.

Nomenclature

Symbols	Meanings	Units
σ	Stress	MPa
ε	Strain	-
$T_{th}/T_{se}/T_{sh}$	Torques at threads/seal surface/torque shoulder	N·m
d	Distance between two points on a rough surface	m
L_c	Self-correlation length	m
R_q	Root-mean-square roughness of surface	m
Q	Volumetric flow rate	$m^3 \cdot s^{-1}$
φ	Flow factor	-
h	Gap between two surfaces	m
p	Pressure of fluid	MPa
Δp	Difference between inlet and outlet pressures	MPa
μ	Viscosity of fluid	kg/(m·s)
b	Width of smooth plate	m
l	Length of smooth plate	m
v	Gas volume	m^3
R	Gas constant	J/(mol·K)
T	Temperature	K
ρ	Gas density	kg/m ³
m	Gas mass	kg
\dot{m}	Mass flow	kg·s ⁻¹
n	Quantity of gas	mole

References

- Hamilton, K.; Wagg, B.; Roth, T. Using ultrasonic techniques to accurately examine seal-surface-contact stress in premium connections. *SPE Drill. Complet.* **2009**, *24*, 696–704. [[CrossRef](#)]
- Han, T.; Fan, J.C. Assessment of stress distribution in premium connections with ultrasonic phased array and metal magnetic memory. *J. Phys. Conf. Ser.* **2021**, *2045*, 012012. [[CrossRef](#)]
- Zhao, L.; Liang, Y.; Zhan, X.; Zhu, W. Investigation of oil casing connection in make-up process and subjected to complex loads. 2023, *under review*.
- Mo, L.; Chen, H.; Tu, L.; Tian, C. Sealing structural design and sealing performance analysis for cylindrical pipe threaded connection. *J. Fail. Anal. Prev.* **2022**, *22*, 1657–1668. [[CrossRef](#)]
- Porcaro, R.R.; Cândido, L.C.; Trindade, V.B.; de Faria, G.L.; Godefroid, L.B. Evaluation of standard API casing connections and parametric API buttress improvement by finite element analysis. *Mater. Res.* **2016**, *20*, 130–137. [[CrossRef](#)]
- Quispe, J.L.P.; Pasqualino, I.P.; Estefen, S.F.; de Souza, M.I.L. Structural behavior of threaded connections for sandwich pipes under make-up torque, external pressure, and axial load. *Int. J. Press. Vessel. Pip.* **2020**, *186*, 104156. [[CrossRef](#)]
- Chen, F.; Di, Q.; Li, N.; Wang, C.; Wang, W.; Wang, M. Determination of operating load limits for rotary shouldered connections with three-dimensional finite element analysis. *J. Pet. Sci. Eng.* **2015**, *133*, 622–632. [[CrossRef](#)]
- Dou, Y.; Li, Y.; Cao, Y.; Yu, Y.; Zhang, J.; Zhang, L. FE simulation of sealing ability for premium connection based on ISO 13679 CAL IV tests. *Int. J. Struct. Integr.* **2020**, *12*, 138–148. [[CrossRef](#)]
- Chen, W.; Di, Q.; Zhang, H.; Chen, F.; Wang, W. The sealing mechanism of tubing and casing premium threaded connections under complex loads. *J. Pet. Sci. Eng.* **2018**, *171*, 724–730. [[CrossRef](#)]

10. Song, F.; Du, M.; Li, K. Numerical and experimental qualification of seal integrity of rotary shouldered connections under combined loads. In *ASME International Mechanical Engineering Congress and Exposition, Proceedings (IMECE)*; American Society of Mechanical Engineers: New York, NY, USA, 2022; Volume 9, p. v009t12a039.
11. Li, Y.; Cao, Y.; Dou, Y.; Yu, Y.; Zhang, J.; Zhang, L. Simulation of sealing ability for premium connection based on ISO 13679 CAL IV tests. *Procedia Struct. Integr.* **2019**, *22*, 43–50. [[CrossRef](#)]
12. Murtagian, G.R.; Fanelli, V.; Villasante, J.A.; Johnson, D.H.; Ernst, H.A. Sealability of stationary metal-to-metal seals. *J. Tribol. Trans. ASME* **2004**, *126*, 591–596. [[CrossRef](#)]
13. Xie, J.; Matthews, C.; Hamilton, A. A study of sealability evaluation criteria for casing connections in thermal wells. In *Proceedings of the SPE Canada Heavy Oil Technical Conference, Calgary, AB, Canada, 7–9 June 2016*.
14. Fischer, F.J.; Schmitz, K.; Tiwari, A.; Persson, B.N.J. Fluid leakage in metallic seals. *Tribol. Lett.* **2020**, *68*, 125. [[CrossRef](#)]
15. Ernens, D.; Pérez-Ràfols, F.; Van Hoecke, D.; Roijmans, R.F.H.; van Riet, E.J.; Voorde, J.B.E.V.; Almqvist, A.; de Rooij, M.B.; Roggeband, S.M.; van Haaften, W.M.; et al. On the sealability of metal-to-metal seals with application to premium casing and tubing connections. *SPE Drill. Complet.* **2019**, *34*, 382–396. [[CrossRef](#)]
16. Greenwood, J.A.; Williamson, J.B.P. Contact of nominally flat surfaces. *Proc. R. Soc. Lond. Ser. A Math. Phys. Sci.* **1966**, *295*, 300–319.
17. Zhao, Y.; Maietta, D.M.; Chang, L. An asperity microcontact model incorporating the transition from elastic deformation to fully plastic flow. *J. Tribol.* **2000**, *122*, 86–93. [[CrossRef](#)]
18. Majumdar, A.; Bhushan, B. Fractal model of elastic-plastic contact between rough surfaces. *J. Tribol.* **1991**, *113*, 1–11. [[CrossRef](#)]
19. Persson, B.N.J. Leakage of metallic seals: Role of plastic deformations. *Tribol. Lett.* **2016**, *63*, 42. [[CrossRef](#)]
20. Zhang, S.; Song, H.; Sandfeld, S.; Liu, X.; Wei, Y. Discrete greenwood–williamson modeling of rough surface contact accounting for three-dimensional sinusoidal asperities and asperity interaction. *J. Tribol.* **2019**, *141*, 121401. [[CrossRef](#)]
21. Xu, H.; Zhang, Z.; Xiang, S.; Yang, B.; Shi, T. Leakage model of tubing and casing premium connection based on sinusoidal contact simulation between rough surfaces. *Processes* **2023**, *11*, 570. [[CrossRef](#)]
22. Yastrebov, V.A.; Anciaux, G.; Molinari, J.-F. On the accurate computation of the true contact-area in mechanical contact of random rough surfaces. *Tribol. Int.* **2017**, *114*, 161–171. [[CrossRef](#)]
23. Shvarts, A.G.; Yastrebov, V.A. Fluid flow across a wavy channel brought in contact. *Tribol. Int.* **2018**, *126*, 116–126. [[CrossRef](#)]
24. Patir, N.; Cheng, H.S. An average flow model for determining effects of three-dimensional roughness on partial hydrodynamic lubrication. *J. Lubr. Technol.* **1979**, *100*, 12–17. [[CrossRef](#)]
25. Persson, B.N.J.; Yang, C. Theory of the leak-rate of seals. *J. Phys. Condens. Matter* **2008**, *20*, 315011. [[CrossRef](#)]
26. Yang, B.; Xu, H.; Xiang, S.; Zhang, Z.; Su, K.; Yang, Y. Effects of make-up torque on the sealability of sphere-type premium connection for tubing and casing strings. *Processes* **2023**, *11*, 256. [[CrossRef](#)]

Disclaimer/Publisher’s Note: The statements, opinions and data contained in all publications are solely those of the individual author(s) and contributor(s) and not of MDPI and/or the editor(s). MDPI and/or the editor(s) disclaim responsibility for any injury to people or property resulting from any ideas, methods, instructions or products referred to in the content.